Materials Science in Semiconductor Processing 72 (2017) 52–59

Contents lists available at ScienceDirect

Materials Science in Semiconductor Processing

journal homepage: www.elsevier.com/locate/mssp

$LiGaTe_2$ (LGT) nonlinear crystal: Synthesis and crystal growth processes exploration

Sergey A. Grazhdannikov[a,*], Pavel G. Krinitsyn[a], Aleksey F. Kurus'[a,b], Ludmila I. Isaenko[a,c,d], Alexander P. Yelisseyev[a], Maksim S. Molokeev[e,f,g]

[a] Sobolev Institute of Geology and Mineralogy, Siberian Branch of Russian Academy of Sciences, 3 Acad. Koptyug Avenue, 630090 Novosibirsk, Russia
[b] Nikolaev Institute of Inorganic Chemistry, Siberian Branch of Russian Academy of Sciences, 3 Acad. Lavrentiev Avenue, 630090 Novosibirsk, Russia
[c] Novosibirsk State University, 2 Pirogova Str., 630090 Novosibirsk, Russia
[d] South Ural State University, 76 Lenin Avenue, 454080 Chelyabinsk, Russia
[e] Kirensky Institute of Physics, Siberian Branch of Russian Academy of Sciences, Akademgorodok Str. 50/38, 660036 Krasnoyarsk, Russia
[f] Far Eastern State Transport University, 47 Serysheva Str., 680021 Khabarovsk, Russia
[g] Siberian Federal University, 79 Svobodny Ave., 660041 Krasnoyarsk, Russia

ARTICLE INFO

Keywords:
$LiGaTe_2$ crystal
Synthesis
Crystal growth
X-ray diffraction
Crystal growth simulation
Optical properties

ABSTRACT

The $LiGaTe_2$ (LGT) single crystal up to 12 mm in size was grown in 3 stages: synthesis, homogenization and crystal growth. The initial charge with 6–10 at% excess of Li_2Te was produced by melting elementary Li, Ga and Te components. The homogenization step was carried out with the maximum value of melt overheating not exceeding 50 K. The Bridgman-Stockbarger technique was used to grow the $LiGaTe_2$ crystals. A furnace of special design, providing the enlargement of LGT linear size, was used. At each stage (synthesis, homogenization and crystal growth) the DTA analysis was carried out: during heating and cooling we recorded peaks corresponding to melting or crystallization of different components in the charge, such as Te^0 (melting point 739 K) and $LiGaTe_2$ (melting point 945 K) and in the as-grown crystal. The XRD analysis was also carried out at each technological stage. The analysis showed that there are 2 side phases (Te^0, Ga_2Te_3), and their phase contents decrease to 1.2 at%, while the $LiGaTe_2$ phase increases up to 93.5 at% during the homogenization process. The synthesized charge composition was analyzed by flame photometry (for Li) and atomic absorption (for Ga and Te). To provide a flat crystallization front and optimal conditions for crystal growth, spatial distribution of thermal field in the furnace was simulated. Transmission spectrum was recorded for the as-grown LGT crystal.

1. Introduction

Search for new nonlinear optical crystals for the mid-infrared is one of the important goals in modern material science. The main requirements for promising nonlinear crystals are a wide transparency range, high nonlinear susceptibility and birefringence. Such crystals are necessary for design of medical devices based on the optical tomography principles, infrared laser spectrometers used for detecting heavy hydrocarbons, in laser targeting systems, etc. Crystals of ternary chalcogenides crystals [1], especially tellurides, are the most promising to generate tunable coherent radiation both in the mid- and far-infrared ranges. The tellurides subgroup has such features as high nonlinear susceptibility and good transparency in the infrared range.

However, the prospects of application of tellurides in nonlinear optics are determined not only by the specified parameters. An important parameter is the birefringence value, which determines the spectral range of the laser radiation conversion. For example, $AgGaTe_2$ crystals have high nonlinear susceptibility of d_{36} = 75 pm/V at λ = 10.6 μm and a broad transparency range from 1 to 18 μm, with very low birefringence Δn = 0.017 and a narrow band gap E_g = 1.32 eV [2,3]. This combination of these properties allows one to realize phase-matching conditions only within a very narrow range of wavelengths. Thus, at room temperature the conversion of CO_2-laser radiation (λ = 10.6 μm) to the second harmonic was obtained only for crystals of mixed composition, where at least 88% of tellurium was replaced by selenium.

It is equally important to achieve a balance between high nonlinear conversion efficiency and band gap. Avanesov et al. [4] obtained a new crystal of $PbIn_6Te_{10}$, which crystallizes in the *R*32 space group. This crystal has high nonlinear susceptibility of d_{36} = 51 pm/V, wide transparency range 1.7–25 μm and average birefringence value Δn = 0.05, but the band gap is narrow: E_g = 1.08 eV. Thus, for this material

* Corresponding author.
E-mail address: grazhdannikovsa@igm.nsc.ru (S.A. Grazhdannikov).

http://dx.doi.org/10.1016/j.mssp.2017.09.017
Received 13 June 2017; Received in revised form 1 September 2017; Accepted 11 September 2017
Available online 28 September 2017

it is necessary to use lasers, emitting in the 2.5–3 μm spectral range as a pump source, and the laser scheme becomes far more complicated.

One of the most promising tellurides is nonlinear crystal $LiGaTe_2$ (LGT), which meets all necessary requirements for effective radiation conversion in the mid-IR range. LGT is characterized by a wide transparency range extending from 0.52 to 17 μm, a large band gap of E_g = 2.4 eV, high nonlinear susceptibility d_{36} = 43 p.m./V, and a high birefringence coefficient of Δn = 0.09 [5]. This unique combination of parameters allows one to realize the frequency conversion in the mid-IR region with efficiency 2 times higher than in the case of well known commercial $AgGaSe_2$ crystal [6].

The LGT powder was obtained by German scientists in 1997 [7]. Since then, there were several attempts to obtain a LGT single crystal of optical quality. In 2003, the first LGT single crystal was grown in IGM (Novosibirsk, Russia), prisms were cut and the Sellmeier equations were established [8]. In 2014, Tupitsyn et al. from USA reported the growth of LGT crystals up to 5 mm in size [9].

The $LiGaTe_2$ crystal has the chalcopyrite structure (*I*-42*d*), which is characterized by the closest face-centered cubic packing of Te. All cations have the coordination number CN = 4 [10]. Half of the tetrahedral cavities are filled with cations Li^+ and Ga^{3+}, the other half of the tetrahedral and all octahedral voids are empty [5,7]. Raman spectroscopy indicates explicit ionic character of Li–Te bonds and covalent one of Ga–Te bonds [11]. In comparison with other lithium chalcogenides, such as $LiGaS_2$ and $LiGaSe_2$, the ionic character of the bond Li-Hal in $LiGaTe_2$ is less pronounced [12]. This duality allows us to explain many of $LiGaTe_2$ properties, as well as some of the features of LGT crystal growth.

The process of LGT crystal growth is complicated by a variety of factors that must be taken into account. The first is that compound includes highly reactive lithium and some volatile components. The compound melts congruently, but above the melting point the incongruent melt evaporation is observed. The latter is the reason for a deviation from the stoichiometric LGT composition in the grown crystal [5]. In addition, at temperature above the melting point, the liquid LGT dissociates to Li_2Te and Ga_2Te_3 with following decomposition into elementary Li^+ and Te^{2-}. Highly reactive Li^+ interacts with the container material and some part of lithium is irretrievably lost. Thereafter, the melt accumulates elementary tellurium and gallium telluride. According to Glazov et al. [13], at temperatures 80–100 K above the melting point, structural changes in gallium telluride take place. The structure with covalent bonds of linear type is supposed to form at these temperatures. This may cause anomalous behavior in density and viscosity of the melt near the crystallization point.

The goal of our study is to investigate the processes of $LiGaTe_2$ synthesis and crystal growth, including the simulation of thermal fields' distribution during the Bridgman-Stockbarger crystallization. We present a series of decisions that allow us to grow larger crystals of optical quality.

2. Experimental

Experiments were conducted in 3 stages: synthesis, homogenization and crystal growth.

2.1. LGT synthesis technique

Synthesis was carried out by melting of elementary initial components Ga and Te (99.999%) and Li (99.99%). The components were charged in graphite glass crucible, which was placed in a quartz reactor with a limited free volume of about 200 cm^3. The reactor connected to the vacuum pump was evacuated at a residual pressure of 10^{-3} Pa and sealed off. Weighing and loading of materials were carried out in a dry box under an argon atmosphere. To avoid deviation from the stoichiometry, we took the charge with up to 16 at% excess of Li and Te. The reactor scheme for synthesis is shown in Fig. 1. To minimize the undesirable effect of strong heating during chemical reaction between lithium and tellurium, at first, the container was placed into the area with a high temperature gradient. As a result, tellurium, as the most volatile component, was transported into the upper, cooler part of the container and the interaction between Te and Li occurred mainly in the gas phase. As a result, local overheating inside the graphite glass crucible with metallic Li decreased significantly. At the end of this stage, because of the intense interaction between components, the temperatures in the upper and lower parts of the container were the same (about 1000 K). The container was kept for a day at this temperature and then cooled to room temperature. After cooling, the container was opened in argon atmosphere and the resulting charge was placed into an ampoule for crystal growth. The synthesized product is a rather dense, dark-gray cryptocrystalline porous aggregate, which is instable in air.

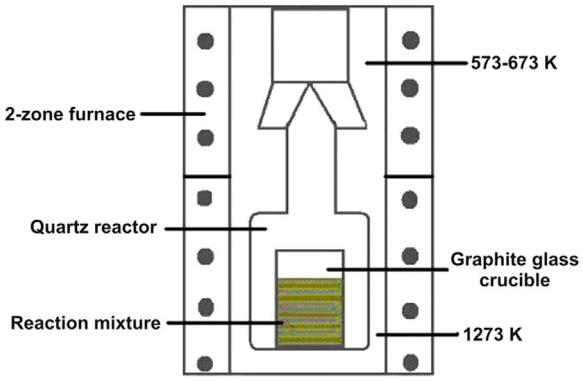

Fig. 1. A scheme of apparatus for $LiGaTe_2$ synthesis.

2.2. Homogenization stage

To obtain a homogeneous charge, an additional stage of charge homogenization was added, the melt overheating during the synthesis was reduced, and the free volume of the ampoule was filled with argon. The homogenization procedure is arranged by alternately reversing rotation of the ampoule with molten synthesized charge at the temperature about 50 K above the LGT melting point [5,13].

2.3. Crystal growth technique

LGT crystals were grown by the Bridgman-Stockbarger technique in a vertical version. We used a two-zone furnace with a diaphragm and a furnace of special design (Fig. 2). The furnace temperature was controlled using a platinum/platinum-rhodium thermocouple and a RPN-4 temperature regulator.

The homogenized charge was placed in a special quartz ampoule with pyrocarbon coating. Afterwards the ampoule was connected to the vacuum pump and the charge was degassed thoroughly. Then free volume of the ampoule was filled with high purity argon, so as to provide the 1 atmosphere pressure at the temperature of crystal growth. An axial temperature gradient of about 2 K/mm was provided in the area of phase boundary. However, this value increases considerably in presence of the heat sink. The ampoule was shifted at a speed of 2.5 mm/day. In our crystal growth experiments we used chromel-alumel thermocouple, because thermocouple of this type provides more accurate temperature measurements. The thermocouple junction was placed on the cone of the crystal growth ampoule on its outer surface. The accuracy of temperature maintenance was ± 0.1 K in the working area. It should be noted that the design of this furnace plays a decisive role in crystal growth. This construction provides a sharp change in the temperature near the crystallization front with a relatively low overheating of the liquid phase. The crystal growth process of LGT crystals occurs in

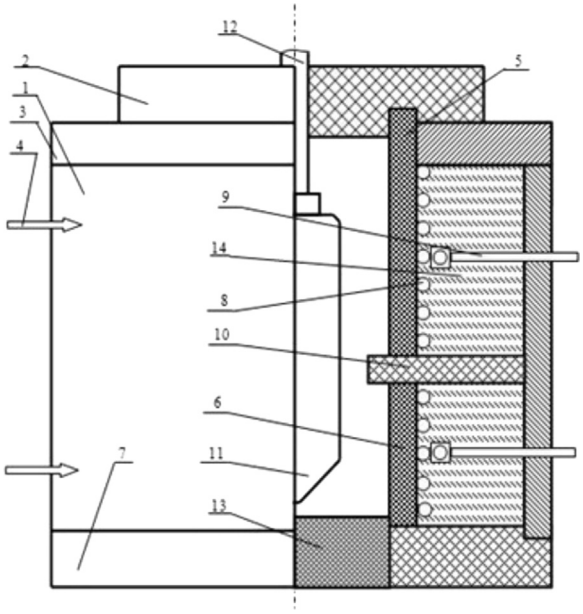

Fig. 2. Design of the furnace for crystal growth, where 1 – furnace body, 2 – chamotte cap, 3-upper flange of the furnace, 4 – thermocouple, 5 – refractory body (upper), 6 – refractory body (lower), 7 – lower flange of the furnace, 8 – heater, 9 – current lead, 10 – diaphragm, 11 – ampoule with melt, 12 – holder, 13 – chamotte plug, 14 – thermal insulation.

the direction {111}, which is typical for the crystals belonging to the space group *I*-42*d*. In growth experiments, at the initial stage the crystal nucleation was observed on the walls of the ampoule, which ultimately affected the shape of the crystal during the crystal growth process. The size of as-grown LGT crystals reached 12 mm. They are zoned in color from light yellow to pink and even red (Fig. 3b, c).

2.4. Chemical analysis

Flame photometry for Li and atomic absorption analysis for Ga and Te were carried out on the Hitachi AA spectrophotometer Z-8000. The relative standard deviation of convergence was about 0.02–0.05.

2.5. DTA technique

DTA analysis was conducted on homemade DTA-analyzer based on the Eurotherm temperature regulator. The heating and cooling rates were 10 K/min.

2.6. The powder diffraction technique

The powder diffraction data for four $LiGaTe_2$ samples for Rietveld analysis were collected at room temperature with a Bruker D8 ADVANCE powder diffractometer (Cu-Kα radiation) and linear VANTEC detector. The step size of 2θ was 0.016°, and the counting time was 0.8 s per step. The 2θ range of 5–70° was measured with a 0.6 mm divergence slit, but 2θ range of 70–140° was measured with a 2 mm divergence slit. Larger slits allow a noticeable increase in the intensity of high-angle peaks without loss of resolution because the high-angle peaks are broad enough to be not affected by a bigger divergence beam. The increase in high-angle peaks intensities led to drastically improved quality of data [14–16] which was proved in several works [17–21]. The esd's $\sigma(I_i)$ of all points on patterns were calculated using intensities I_i: $\sigma(I_i) = I_i^{1/2}$. The intensities and obtained esd's were further normalized: $I_{i\ norm} = I_i \times 0.6/(\text{slit width})$, $\sigma_{norm}(I_i) = \sigma(I_i) \times 0.6/(\text{slit width})$, taking into account the actual value of divergence slit width

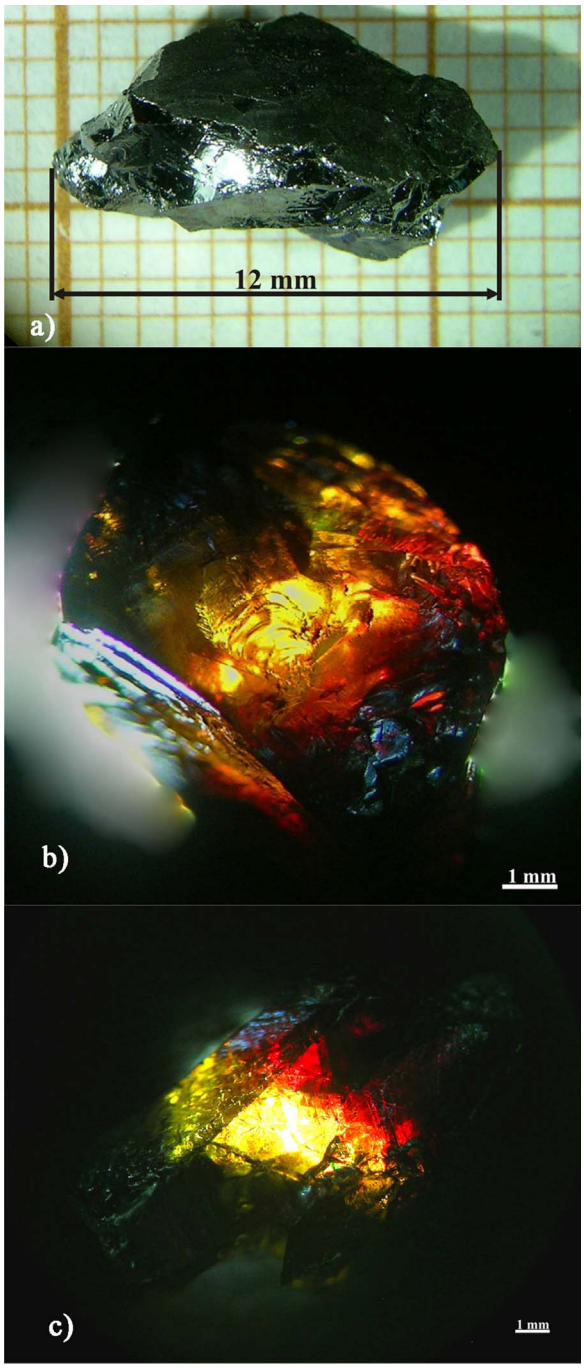

Fig. 3. Three as-grown LGT crystals (a-c) up to 12 mm in size. Patterns were obtained at side illumination (a) and in transmitted light (b-c). (For interpretation of the references to color in this figure, the reader is referred to the web version of this article.)

which was used to measure each particular intensity I_i, and saved in xye-type file. So the transformed powder pattern has a typical view in the whole 2θ range 5–140°, but all high-angle points have small esd's [14–16].

2.7. Modeling of crystal growth process

A model of the crystal growth process was built in the STR Crystal Growth Simulation package (CGSim rev.16.1). This package allows simulating heat and mass transfer phenomena occurring in the Bridgman-

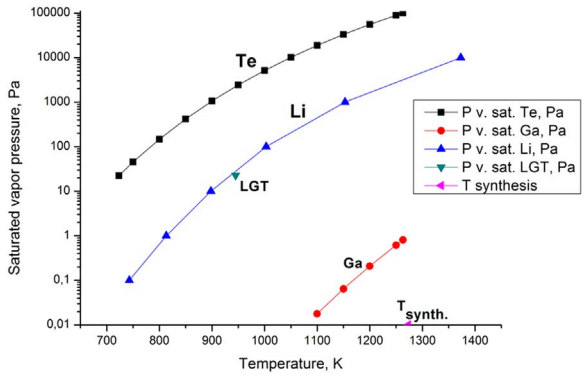

Fig. 4. Temperature dependence of Te, Li, Ga partial pressures and on the vapor pressure of $LiGaTe_2$.

Stockbarger, Czochralski, LEC and HEM processes of crystal growth.

2.8. Transmission spectrum

Transmission spectra were recorded using a UV-2501 PC Shimadzu spectrometer in the UV to near IR, whereas in the mid-IR we used a Fourier transform spectrometer Infralum 801.

3. Results and discussion

3.1. LGT synthesis

At synthesis temperature about 1273 K, the partial pressures of volatile components (Li and Te) were significant, whereas vapor pressure of $LiGaTe_2$ compound was negligible (less than 1 mm of mercury column) (Fig. 4).

The temperature dependences for saturated vapor pressure of Te and Ga were calculated according to the following formulas from [22,23]:

$$\lg P_{Te_l}(mmHg) = 6.402 - \frac{6016}{T} + 0.400 \lg T\,(723 - 1263K)$$

$$\lg P_{Ga_l}(hPa) = 1.1277 - \frac{13425.42}{T} - 6.0331\cdot10^{-4}T + 2.95655 \lg T$$

Temperature dependence of Li saturated vapor pressure was built using data from [24]. The melting point for $LiGaTe_2$ (T_m = 945 K) was determined by Prof. Vasilyeva during the investigation of the boiling points and also in direct measurements [25,26].

Thus, the vapor pressure of the LGT compound was found to be extremely small: major parts of vapor are the products of incongruent evaporation. In order to compensate incongruent evaporation and dissociation, it is necessary to limit the melt overheating (not more than 50 K above the melting point), as well as to provide additional pressure when introducing Ar into the ampoule free volume.

DTA experiments showed that synthesized charge was inhomogeneous. On the heating curve we found the main peak near 945 K interpreted as a melting point T_m for the $LiGaTe_2$ phase and a weak additional peak near 739 K, related to the Te^0 phase (Fig. 5) [27]. Similar peaks were also observed on cooling. In the latter case, we observed another additional peak near 845 K, associated with the $Li_2Si_2O_5$ silicate phase. DTA experiments were carried out using a crucible without carbon coating and silicate phase appeared as a result of melt interaction with the walls of the silica ampoule.

The charge composition after the synthesis was determined by flame photometry (for Li) and atomic absorption (for Ga and Te). The composition obtained from the analysis of samples from different parts of the ingot corresponds to the following formulas: $Li_{0.79}GaTe_{2.11}$, $Li_{1.37}GaTe_{1.92}$, $Li_{0.84}GaTe_{2.23}$, $Li_{1.86}GaTe_{2.23}$, $Li_{0.75}GaTe_{1.99}$ (Ga concentration is taken as 1).

Li deficiency in four of these samples was a result of Li interaction with the container walls during the synthesis. Excessive Li_2Te and Te^0 contents were due both the original excess of Li and Te in the charge after loading and the disproportionation according to the scheme $Ga_2Te_3 \rightarrow GaTe + Te$ in case of fluid overheating [13]. According to the obtained results, the Li_2Te excess was reduced to 6–10 at%.

Thus, the synthesized LGT charge was shown to be neither homogeneous nor single phase. To obtain a homogeneous charge, an additional stage of charge homogenization was added. DTA of produced ingot showed no signal from the Te^0 side phase, which confirmed the efficiency of melt homogenization step.

Crystal structure refinement was performed using DDM (Derivative Difference Minimization) program [28] which accounts esd's of each point by special weight scheme. Almost all diffraction peaks besides small amount of impurity peaks (~ 4% Te and ~ 3% Ga_2Te_3) were indexed by tetragonal cell ($I-42d$) with parameters close to $LiGaTe_2$ [29], and therefore this crystal structure was taken as the starting model for refinement. Refinements were stable and gave low R-factors (Table 1, Fig. 6). Coordinates of atoms are in Table 2.

The XRD analysis shows the presence of Ga_2Te_3 in the synthesized (**1**, **2**) and homogenized (**3**, **4**) charges, while on the DTA heating curve near T = 1063 K there is a low pronounced feature [27]. It is worth noting that homogenization process results in lowering of Te^0 and Ga_2Te_3 phase content up to 1.2 at%, while the $LiGaTe_2$ phase increases up to 93.5 at%.

3.2. Growth of LGT crystals

As-grown LGT crystals were analyzed by DTA. The results of DTA analysis for obtained LGT crystals are given in Fig. 7. One can see a single peak on the heating curve (T = 943 K, at left), and a peak near T = 954.5 K on the cooling curve, which is associated with the $LiGaTe_2$ phase (at right). In contrast to the synthesized charge, there is no peak associated with the $Li_2Si_2O_5$ phase in curves for crystal DTA: this is a result of graphite coating in the case of the ampoule for the crystal growth.

3.3. Thermal field simulation

To understand why crystals form on the walls of the vial and how to change the thermal field to control the process, we simulated the temperature gradients in conditions close to the experimental ones. Crystal nucleation on the walls of the ampoule may be due to a concave shape of the interface during crystal growth. To estimate the influence of thermal field distribution on the interface shape, the mathematical model of the global heat transfer in the furnace was used. Heat transfer by thermal conductivity, and convection was taken into account in such calculations. Radiative heat transfer was not taken into account because of the lack of data on LGT emissivity. The following thermal parameters of solid and melted LGT were used:

Thermal conductivity of LGT crystal, W/m K	4.5 [30]
Thermal conductivity of LGT melt, W/m K	≈ 8 [31]
Melting point, K	943 (from DTA)
Latent heat, kJ/kg	≈ 31.8 (from DTA)
Heat capacity of the crystal C_P = 100.01 + 0.0219·T – 191210·T^{-2} J/mol K [32]	

Since the LGT melt is prone to lamination, it is assumed that the thermal conductivity of the LGT melt is mainly determined by the thermal conductivity of the tellurium melt [31]. The calculation does not take into account the convection in the melt because the volume

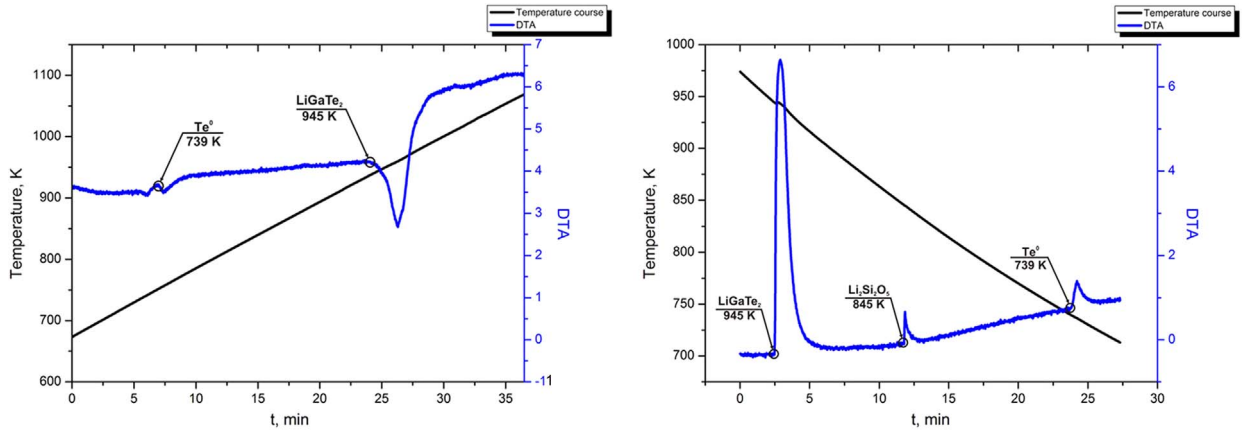

Fig. 5. DTA results obtained on heating (at left) and cooling (at right) of the synthesized charge. The peaks at 739, 845 and 945 K are related to Te^0, $Li_2Si_2O_5$ and $LiGaTe_2$, respectively.

Table 1
Main parameters of processing and refinement of the $LiGaTe_2$ (**1–4**) samples.

Compound	Phase	Weight (%)	Space group	Cell parameters (Å, °), Cell volume (Å^3)	R_{wp}, R_p, $R_{B(\text{main phase})}$ (%)
(1)	$LiGaTe_2$	93 (1)	*I*-42*d*	*a* = 6.33696 (5) *c* = 11.6986 (1) *V* = 469.781 (8)	8.77, 5.17, 4.31
	Te	4 (1)	$P3_121$	*a* = 4.457 (1) *c* = 5.923 (3) *V* = 101.88 (8)	
	Ga_2Te_3	3.0 (2)	*F*-43*m*	*a* = 5.87358 (6) *V* = 202.633 (6)	
(2)	$LiGaTe_2$	92 (1)	*I*-42*d*	*a* = 6.33695 (4) *c* = 11.6972 (1) *V* = 469.715 (7)	10.10, 5.54, 4.79
	Te	4.4 (3)	$P3_121$	*a* = 4.460 (5) *c* = 5.923 (4) *V* = 102.0 (2)	
	Ga_2Te_3	3.3 (1)	*F*−43*m*	*a* = 5.87134 (5) *V* = 202.410 (6)	
(3)	$LiGaTe_2$	93 (1)	*I*−42*d*	*a* = 6.33876 (4) *c* = 11.70024 (9) *V* = 470.108 (7)	10.62, 5.84, 5.34
	Te	3.2 (5)	$P3_121$	*a* = 4.43700 (3) *c* = 5.90499 (4) *V* = 100.674 (1)	
	Ga_2Te_3	3.8 (3)	*F*-43*m*	*a* = 5.8777 (2) *V* = 203.04 (2)	
(4)	$LiGaTe_2$	93.5 (10)	*I*-42*d*	*a* = 6.33900 (4) *c* = 11.7007 (1) *V* = 470.131 (7)	9.82, 6.39, 5.92
	Te	3.9 (1)	$P3_121$	*a* = 4.43748 (2) *c* = 5.90569 (3) *V* = 100.703 (1)	
	Ga_2Te_3	2.6 (1)	*F*-43*m*	*a* = 5.8789 (2) *V* = 203.15 (2)	

and column height of the melt are small: thus, the influence of these phenomena can be neglected.

Fig. 8 shows the spatial distribution of thermal fields and the shape of the melting isotherm inside the growth ampoule. The estimated average value of radial temperature gradient dT/dx inside crystal reaches $0.1{\cdot}10^{-3}$ K/m (Fig. 9). The areas of local inhomogeneity in the thermal field inside crystal, where the radial temperature gradient reaches $0.4{\cdot}10^{-3}$ K/m, are marked. This feature of the temperature distribution results in the increase in the internal thermoelastic stresses in the crystal [33]. Axial gradient dT/dy in the crystal varies from $8{\cdot}10^{-3}$ to $2.9{\cdot}10^{-3}$ K/m (Fig. 10). Basing on model assumptions, recommendations for the furnace design were given. The calculations show a concave front of crystallization and 50 K melt overheating above melting temperature. There is a lamination of the LGT melt when melt overheating exceeds this value (50 K).

3.4. LGT transmission

Fig. 11 shows the transmission spectrum LGT sample 250 μm thick, recorded at room temperature. One can see that LGT crystal is transparent in the 0.495–18 μm spectral range (curve 1 in Fig. 10). Curve 2 shows the absorption spectrum calculated from the transmission spectrum. Initially the transmission increases sharply in the 0.495–0.550 μm range, then transmission grows more slowly and the increase becomes

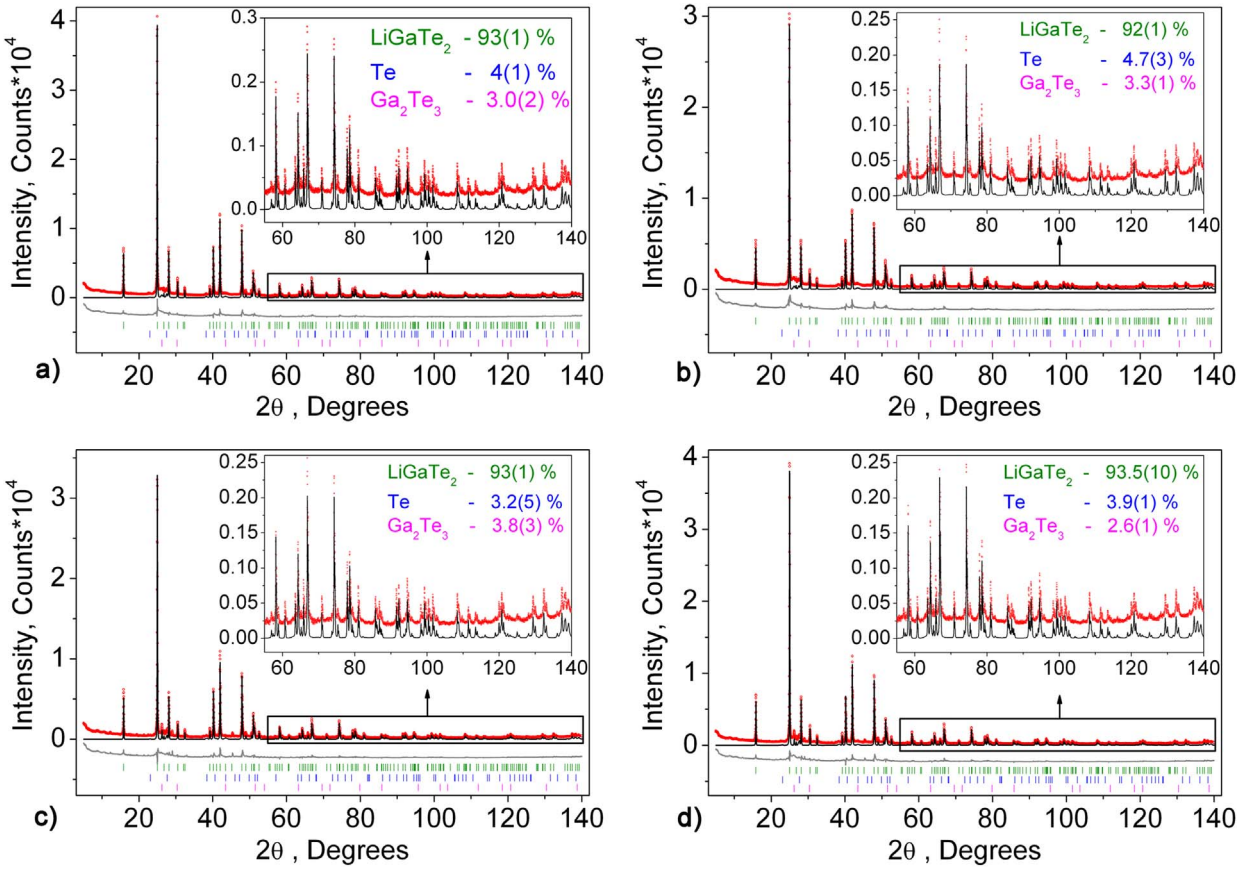

Fig. 6. Difference Rietveld plot of (**1–4**) samples: panels (a – d), respectively. Red dots show observed powder data Y_{obs}, whereas black line shows the calculated pattern Y_{calc}. Gray line below is the difference Y_{obs}–Y_{calc}. Colored sticks depict Bragg peak positions of each corresponding phase. (For interpretation of the references to color in this figure legend, the reader is referred to the web version of this article.)

Table 2
Fractional atomic coordinates and isotropic displacement parameters (Å^2) of $LiGaTe_2$ (**1–4**) samples.

	x	*y*	*z*	U_{iso}
(1)				
Te	0.2668 (3)	3/4	1/8	0.0152 (5)
Ga	0	0	1/2	0.015 (1)
Li	0	0	0	0.21 (7)
(2)				
Te	0.2677 (4)	3/4	1/8	0.0109 (4)
Ga	0	0	1/2	0.012 (3)
Li	0	0	0	0.04 (3)
(3)				
Te	0.2675 (3)	3/4	1/8	0.0111 (3)
Ga	0	0	1/2	0.009 (1)
Li	0	0	0	0.02 (2)
(4)				
Te	0.2681 (3)	3/4	1/8	0.0143 (5)
Ga	0	0	1/2	0.016 (1)
Li	0	0	0	0.13 (6)

slightly pronounced in the 3–12 μm spectral range. The sharp transmission increase at short wavelength is due to the band-to-band absorption.

In [11] the values of the LGT band gap E_g = 2.65 and 2.41 eV at 80 and 300 K, respectively, were estimated. The Tauc analysis showed that the band gap is determined by direct allowed transitions. Increase in the range from visible to 3 μm is due to the Rayleigh light scattering. This scattering is maximal at short wavelengths and decreases as $1/\lambda^4$ as the wavelength grows. The broad absorption band is observed around 17 μm. The 8 μm band is also widespread in Li ternary chalcogenides and also in chalcogenide glasses where this band is related to vibrations with participation of impurity atoms such as Ge-O [34]. We associate the Ge impurity, which was got into the charge during the placement of the components into the graphite glass crucible before the synthesis. The LGT Raman scattering spectra demonstrate the vibrations in the range of 70–350 cm^{-1} [11], wherein the most intense Raman line is near 120 cm^{-1}. Thus, the intense absorption band, which determines the transparency edge position in the mid-IR for the bulk LGT crystals, corresponds to two-phonon absorption in the crystal lattice.

4. Conclusions

The optimal charge composition for growing LGT single crystals of optical quality was established taking into account the high Li chemical activity and Te volatility: 6–10 at% excess for Li and Te over the stoichiometric composition. The composition optimization was carried out using flame photometry techniques for Li, and atomic absorption for Ga and Te, as well as DTA. We improved the LGT crystal growth method: now it consists of 3 phases such as synthesis, homogenization and the Bridgman-Stockbarger crystal growth. Large LGT crystals up to 12 mm in size were obtained. The transmission spectrum for the 250 μm thick LGT plate was recorded.

Spatial distribution of thermal field was simulated using the global

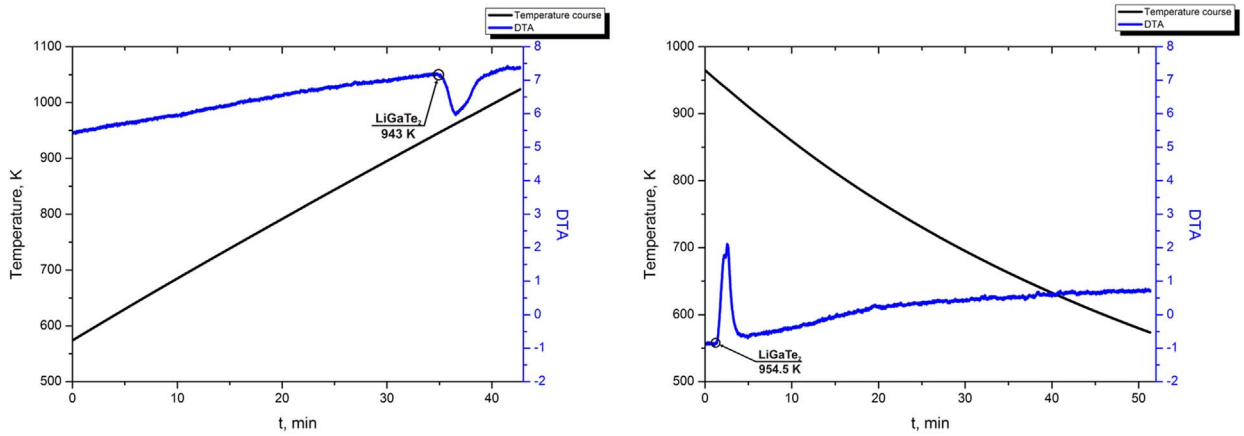

Fig. 7. DTA results for LGT crystal: the heating curve with a peak near 943 K at left and the cooling curve beginning from the melting point, with a peak near 954.5 K, at right.

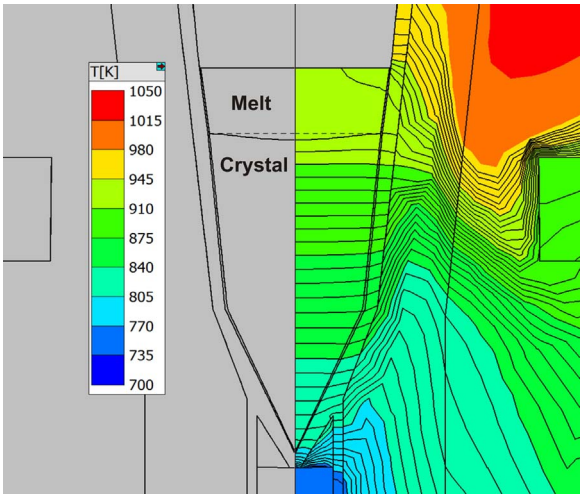

Fig. 8. Spatial distribution of temperature in the furnace.

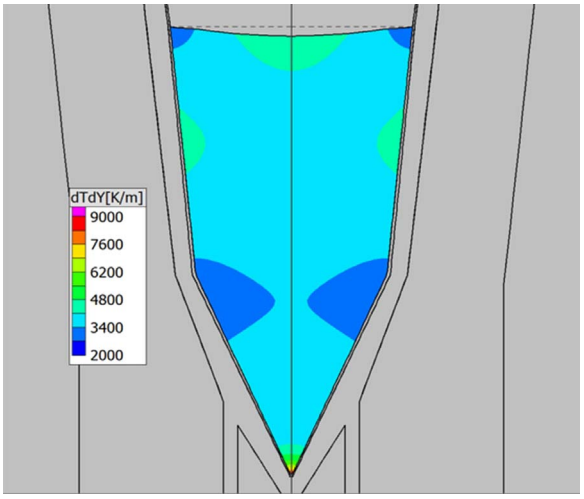

Fig. 10. Spatial distribution of temperature gradient in the crystal.

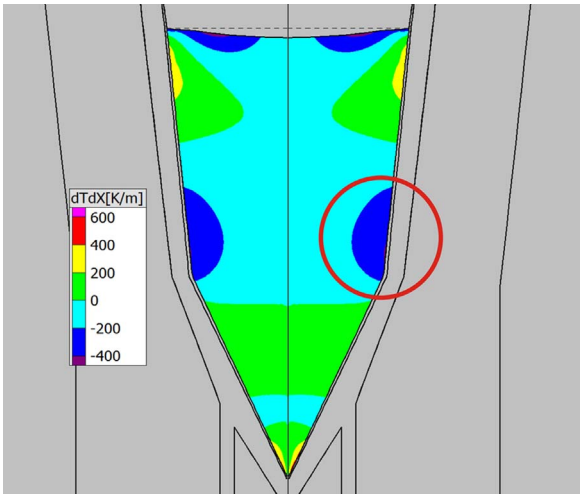

Fig. 9. Spatial distribution of temperature gradient in the crystal. The areas of local inhomogeneity in thermal field inside crystal are marked.

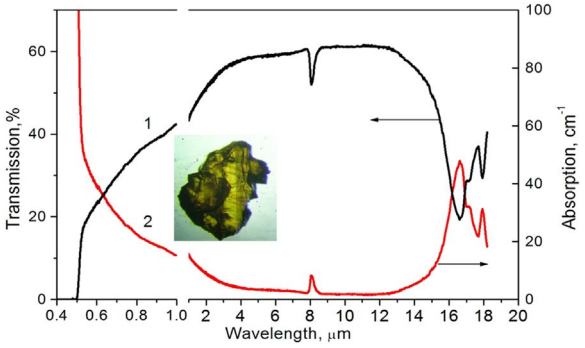

Fig. 11. Transmission (1) and absorption (2) spectra for 250 μm thick LGT sample. In the insert: LGT sample, for which the spectrum was recorded.

heat transfer model. We showed that the LGT crystal grows with a concave crystallization front and there are areas with a high thermal stress inside the crystal. Thermal conditions for LGT crystal growth, providing maximal yield of single crystal material were recommended.

Acknowledgements

This work was supported by the Russian Foundation for Basic Research (Grant no. 15-02-03408a), by the Ministry of Education and Science of the Russian Federation (# 4.1346.2017/4.6), by Act 211 of the Government of the Russian Federation (Contract # 02.A03.21.0011) and by State Assignment Project (# 0330-2016-0009). The authors also thank D. A. Nagorskiy for help with DTA and N. F. Beyzel and A. R. Tsygankova for help in chemical analysis.

References

[1] Z.Z. Kish, E.Yu Peresh, V.B. Lazarev, E.E. Semrad, Systematics and the rules of variations in the properties of $A^{I}B^{III}C_2^{VI}$–type compounds, Inorg. Mater. 23 (1987) 697–703.

[2] P.G. Shunemann, S.D. Setzler, T.M. Pollak, M.C. Ohmer, J.T. Goldstein, D.E. Zelmon, Crystal growth and properties of $AgGaTe_2$, J. Cryst. Growth 211 (2000) 242–246.

[3] K. Aravinth, G. Anandha Babun, P. Ramasamy, Silver gallium telluride ($AgGaTe_2$) single crystal: synthesis, accelerated crucible rotation-Bridgman growth and characterization, Mater. Sci. Semicond. Process. 24 (2014) 44–49.

[4] S. Avanesov, V. Badikov, A. Tyazhev, D. Badikov, V. Panyutin, G. Marchev, G. Shevyrdyaeva, K. Mitin, F. Noack, P. Vinogradova, N. Schebetova, V. Petrov, A. Kwasniewski, $PbIn_6Te_{10}$: new nonlinear crystal for three-wave interactions with transmission extending from 1.7 to 25 μm, Opt. Mater. Express 7 (2011) 1286–1291.

[5] L. Isaenko, I. Vasilyeva, A. Merkulov, A. Yelisseyev, S. Lobanov, Growth of new nonlinear crystals $LiMX_2$ (M = Al,In,Ga; X = S,Se,Te) for the mid-IR optics, J. Cryst. Growth 275 (2005) 217–223.

[6] L. Isaenko, P. Krinitsin, V. Vedenyapin, A. Yelisseyev, A. Merkulov, J.J. Zondy, V. Petrov, $LiGaTe_2$: a new highly nonlinear chalcopyrite optical crystal for the mid-IR, Cryst. Growth Des. 5 (2005) 1325–1329.

[7] J. Brückner, I-III-VI-Verbindungshalbleiter mit Lithium als Gruppe I-Element: Kristallzüchtung and Charakterisierung, Dissertation, Albert-Ludwigs-Universität, Freiburg i. Br, Germany, 1997.

[8] J.-J. Zondy, F. Bielsa, A. Douillet, L. Hilico, O. Acef, V. Petrov, A. Yelisseyev, L. Isaenko, P. Krinitsin, Frequency doubling of CO_2 laser radiation at 10.6 μm in the highly nonlinear chalcopyrite $LiGaTe_2$, Opt. Lett. 12 (2007) 1722–1724.

[9] E. Tupitsyn, P. Bhattacharya, E. Rowe, L. Matei, Y. Cui, V. Buliga, M. Groza, B. Wiggins, A. Burger, A. Stowe, Lithium containing chalcogenide single crystals for neutron detection, J. Cryst. Growth 393 (2014) 23–27.

[10] A.A. Godovikov, Mineralogy, Nedra, Moscow, 1983, pp. 89–90 (in Russian).

[11] A. Yelisseyev, P. Krinitsin, L. Isaenko, S. Grazhdannikov, Spectroscopic properties of nonlinear optical $LiGaTe_2$ crystal, Opt. Mater. 42 (2015) 276–280.

[12] L.I. Isaenko, A.P. Yelisseyev, Recent studies of nonlinear chalcogenide crystals for the mid-IR, Semicond. Sci. Technol. 31 (2016) 24.

[13] V.M. Glazov, S.N. Chizhevskaya, N.N. Glagoleva, Liquid Semiconductors, Nauka, Moscow, 1967, pp. 104–106 (in Russian).

[14] I.C. Madsen, R.J. Hill, Variable step-counting times for Rietveld analysis or getting the most out of your experiment time, Adv. X-ray Anal. 35 (1992) 39–47.

[15] I.C. Madsen, R.J. Hill, Collection and analysis of powder diffraction data with near-constant counting statistics, J. Appl. Cryst. 27 (1994) 385–392.

[16] K. Laursen, T. White, Rietveld refinement of 2-theta split ranges–a method for reducing analysis time, Adv. X-Ray Anal. 46 (2003) 220–225.

[17] M.S. Molokeev, E.V. Bogdanov, S.V. Misyul, A. Tressaud, I.N. Flerov, Crystal structure and phase transition mechanisms in $CsFe_2F_6$, J. Solid State Chem. 200 (2013) 157–164.

[18] N.N. Golovnev, M.S. Molokeev, Crystal structure of catena-DI(2-thiobarbiturato-O,S)aqualead(II), J. Struct. Chem. 54 (5) (2013) 968–971.

[19] M.S. Molokeev, S.V. Misjul, I.N. Flerov, N.M. Laptash, Reconstructive phase transition in $(NH_4)_3TiF_7$ accompanied by the ordering of TiF6 octahedra, Acta Cryst. B 70 (6) (2014) 924–931.

[20] N.N. Golovnev, M.S. Molokeev, Crystal structures of cesium and rubidium 2-thiobarbiturates, Russ. J. Inorg. Chem. 59 (9) (2014) 943–946.

[21] N.N. Golovnev, M.S. Molokeev, Crystal structure of catena-(2-thiobarbiturato) dithallium(I), J. Struct. Chem. 55 (1) (2014) 125–129.

[22] Chemical Encyclopedia: Volume 1, edited by I.L. Knunyants, Moscow, 1988, p. 479 (in Russian).

[23] Chemical Encyclopedia: Volume 4, edited by N.S. Zefirov, Moscow, 1995, p. 514 (in Russian).

[24] S. Weise, Züchtung und Characterisierung von Kristallen in System Li_2Se – In_2Se_3, Dissertation, Aachen, Germany, 2002.

[25] Ya.I. Gibner, I.G. Vasillyeva, Rapid heating in high-temperature thermo-microscopic analysis, J. Therm. Anal. 53 (1998) 151–160.

[26] I.G. Vasilyeva, R.E. Nikolaev, P.G. Krinitsin, L.I. Isaenko, Phase transitions of nonlinear optical $LiGaTe_2$ crystals before and after melting, J. Phys. Chem. C 121 (2017) 17429–17435.

[27] D.M. Chizhikov, V.P. Schastliviy, Tellurium and Tellurides, Nauka, Moscow, 1966, p. 280 (in Russian).

[28] L.A. Solovyov, Full-profile refinement by derivative difference minimization, J. Appl. Crystallogr. 37 (2004) 743–749.

[29] W. Hönle, G. Kühn, H. Neumann, Die KristallStruktur von $LiInTe_2$, Z. Anorg. Allg. Chem. 532 (1986) 150–156.

[30] L. Isaenko, A. Yelisseyev, S. Lobanov, P. Krinitsin, V. Petrov, J.-J. Zondy, Ternary chalcogenides $LiBC_2$ (B=In, Ga; C=S, Se, Te) for mid-IR nonlinear optics, J. Non-Cryst. Solids 352 (2006) 2439–2443.

[31] Sh Zhu, C. Li, Ch-H. Su, B. Lin, H. Ban, R.N. Scripa, S.L. Lehoczky, Thermal diffusivity,thermal conductivity,and specific heat capacity measurements of molten tellurium, J. Cryst. Growth 250 (2003) 269–273.

[32] V.A. Drebushchak, L.I. Isaenko, S.I. Lobanov, P.G. Krinitsin, S.A. Grazhdannikov, Experimental heat capacity of $LiInS_2$, $LiInSe_2$, $LiGaS_2$, $LiGaSe_2$ and $LiGaTe_2$ from 180 to 460 K, J. Therm. Anal. Calorim. 129 (2016) 103–108.

[33] W.C. Dash, Copper precipitation on dislocations in silicon, J. Appl. Phys. 27 (1956) 1193–1195.

[34] V.F. Kokorina, Glasses for Infrared Optics, CRCPress, Boca Raton, USA, 1996.